2026 IEEE International Conference on Robotics and Automation (ICRA 2026)
June 1-5, 2026. Vienna, Austria

Analytical Stiffness Formulation and Interpretation for Six-DOF Tensegrity Joints Using Screw Theory

Robbie Monke[1], and Vishesh Vikas[1]

***Abstract*—Compliant mechanisms, e.g., tensegrities, inherently exhibit nonlinear behavior, wherein the stiffness matrix, evaluated at a specific configuration, characterizes the instantaneous relationship between applied forces and resulting displacements. For traditional robot joints, the stiffness matrix is defined using Cartesian and Euler angle parameters. This representation is convenient when the joints display translation or single degree of rotation behavior, e.g., revolute or prismatic joints. However, it faces parameterization issues in modeling higher degree of freedom joints due to singularities and lack of uniqueness. Lie groups and screw theory representations provide a minimal and intrinsic representation of the rigid body motion. This representation is well suited for tensegrity joints which combine tensile and compressive members and behave as six degree-of-freedom joints. A key challenge in this context is that computing the stiffness matrix necessitates differentiating the transformation matrix (exponential of a screw matrix, i.e., Lie Group) with respect to the screw (Lie algebra), a task that is highly nontrivial. This work derives an analytical formulation of the stiffness matrix for six degree-of-freedom tensegrity joints using screw theory representation, including a closed-form expression for the derivative of the transformation matrix with respect to its screw coordinates. The analytical results are validated against numerical differentiation with agreement to within numerical precision while achieving approximately three times faster computation speeds. Additionally, simulation of the tensegrity subvertebrae was performed applying compressive and rotational loading conditions, confirming accuracy to analytical derivative predictions with errors below 1% and reducing the computation time by a factor of 3. The paper further interprets the stiffness matrix through block-form, column-wise, and row-wise representations, providing additional physical insight into the translational, rotational, and coupled stiffness contributions. These contributions establish an efficient framework for the stiffness analysis and lay the foundation for future integration of screw theory methods into Euler-Lagrange dynamics for higher degree-of-freedom robot joints including tensegrity joints.**

***Index Terms*—Kinematics, tensegrity mechanisms, 6-DOF joint, stiffness Matrix, Lie group, Lie algebra, compliant joints**

I. Introduction

Tensegrity structures are pre-stressed systems that synergistically combine tensile elements and compressive rigid components to maintain the mechanism's structural integrity. These structures have been found to have many benefits in comparison to traditional robot mechanisms due to their compliant nature, packability, impact resistance, and high strength-to-weight ratios [1]–[4]. These features make them attractive for applications in space robotics, robotic manipulation, and biomechanical systems. Consequently, researchers have developed tensegrity joints that mimic traditional rigid robot joints. For example, Lessard et al. developed an actuated two DOF tensegrity elbow joint [5]. Hao et al. created a two DOF joint for applications of ultrasound robotic manipulators [6], [7]. Chen et al. proposed a design methodology for a three DOF joint that was validated through simulation and experimental results [8]. However, modeling the kinematics and dynamics of these systems is challenging due to the antagonistic interaction between their compressive and tensile members.

The stiffness matrix of tensegrity systems allows insight into the structural response of the system to changes in its morphology, actuation, or external loads. For example, Hao et al. used the stiffness matrix to apply dynamic stiffness control to a manipulator end-effector joint [6], [7]. Zhang et al. developed a form-finding method by iteratively calculating the stiffness matrix and the corresponding nodal positions of the structure until the equilibrium configuration was confirmed [9]. Savin et al. proposed an algorithm to develop the desired compliance using convex optimization of the stiffness matrix [10]. Stiffness matrices for tensegrity systems are traditionally calculated using the equations of equilibrium for the external forces at each of the nodes of the structure and then differentiating these forces with respect to movement of the nodes [11], [12]. This formulation can be seen implemented on a tensegrity joint specifically in the two DOF joint by Hao et al. [6], [7]. While this approach allows for a simple and intuitive visualization of stiffness of the system, issues arise when modeling joints of higher degrees of freedom. In higher degree-of-freedom joints, the Euler angles become poorly parameterized as they are non-unique and order dependent.

Screw theory provides a more robust mathematical framework by representing motion and forces as twists and wrenches along a screw axis. Unlike Cartesian and

*This work was supported in part by USDA/NIFA Award #2023-67022-40918, NSF Award #2452608, 2344385.

[1]Robbie Monke and Vishesh Vikas are with the Agile Robotics Lab, University of Alabama, Tuscaloosa, AL 35487, USA rrmonke@crimson.ua.edu, vvikas@ua.edu

Euler formulations, screw theory explicitly represents the translation and rotation of the motion through geometric approach, avoids parameterization issues, and provides a compact representation to be used in kinematics and dynamics [13]–[15]. These benefits make it well suited to be used for tensegrity joints, where multiple degrees of freedom must be modeled consistently. The use of screw theory allows for proper characterization of the movement, stiffness, and forces of the system, resulting in improved design and control of tensegrity joints.

In addition to its utility for the kinematical representation, the integration of screw theory in Euler-Lagrange dynamics provides a consistent framework where the generalized coordinates correspond to the screw representation of the rigid body motion [16]. However, when modeling higher degree of freedom joints using Euler-Lagrange dynamics, the solution will require the differentiation of the exponential of the skew symmetric matrix, $\widehat{\boldsymbol{\xi}}$, with respect to the generalized coordinates, the screw $\boldsymbol{\xi}$. This mathematical step is highly non-trivial to obtain, and to the best of the authors' knowledge an analytical solution has not been shown in literature.

Contributions: Here, we derive an analytical solution for the stiffness matrix of a tensegrity joint using a screw theory-based modeling framework. In the process, a closed-form solution for the derivative of the transformation matrix with respect to its screw coordinates is developed. This finding provides the foundation for future work in screw theory dynamics formulations. The results given by the derivations were validated through two methodologies. First, the analytical solutions were confirmed by comparison to the numerical differentiation methods, which shows full agreement for 10000 configuration states. The computational time is compared between the analytical and numerical solutions, showing the analytical solutions to be approximately 3 times faster than the numerical counterparts. Additionally, the calculated stiffness matrix is compared with that calculated using energy-minimization form-finding method to simulate the response of a tensegrity joint to perturbation forces.

The paper is structured as follows: Section II presents the screw theory based modeling framework used. Section III outlines the closed-form solution of the stiffness matrix derivation. Section IV shows the analytical solution of the derivative of the transformation matrix with respect to its screw coordinates. Section V provides insight into multiple physical interpretations of the structure of the stiffness matrix. Finally, Section VI presents the comparisons of closed form solutions with the numerical differentiation and simulation results.

II. Modeling Framework

The tensegrity mechanism discussed here is composed of two curved rigid links connected by twelve strings. The relative motion between the two links is represented by a screw motion, $\boldsymbol{\xi} \in \mathbb{R}^6$. The corresponding homogeneous transformation relating coordinate systems $\{2\}$ to $\{1\}$ fixed on the two links is

$$T(\boldsymbol{\xi}) = \exp(\widehat{\boldsymbol{\xi}}) \in SE(3), \quad \boldsymbol{\xi} = \begin{bmatrix} \boldsymbol{\omega} \\ \boldsymbol{v} \end{bmatrix} \mathbb{R}^{6\times 1}$$
$$\widehat{\boldsymbol{\xi}} = \begin{bmatrix} 0 & -\omega_3 & \omega_2 & v_1 \\ \omega_3 & 0 & -\omega_1 & v_2 \\ -\omega_2 & \omega_1 & 0 & v_3 \\ 0 & 0 & 0 & 0 \end{bmatrix} \in \mathfrak{se}(3) \tag{1}$$

where the operator $\wedge : \mathbb{R}^{6\times 1} \to \mathfrak{se}(3)$. The reader may refer to Murray et al. [13] for details of the notation adopted in this paper. For transformations involving rotations with constant velocity over time, $\theta = |\boldsymbol{\omega}|$ is the magnitude of motion, the unit vector $\boldsymbol{u} = \boldsymbol{\omega}/\theta \in \mathbb{R}^3$ defines the direction of the screw axis, while $\boldsymbol{v} \in \mathbb{R}^3$ determines its spatial location of the axis of rotation and pitch of the screw motion. Geometrically, the transformation corresponds to a rotation of magnitude θ about the screw axis along $\boldsymbol{u}$ passing through a point $\boldsymbol{\rho}$ together with a translation of magnitude $h\theta$ along $\boldsymbol{u}$. Here, $\boldsymbol{\rho}$ can be obtained from $\boldsymbol{v} = -\widehat{\omega}\boldsymbol{\rho} + h\boldsymbol{\omega}$. A geometric interpretation is illustrated in Fig. 1 and

$$T(\boldsymbol{\xi}) = \begin{bmatrix} \exp(\widehat{\boldsymbol{\omega}}) & G(\theta)\boldsymbol{v} \\ \mathbf{0} & 1 \end{bmatrix}, \text{ s.t. } \theta = |\boldsymbol{\omega}| \tag{2}$$

$$\exp(\widehat{\boldsymbol{\omega}}) = I + \frac{s_\theta}{\theta}\widehat{\boldsymbol{\omega}} + \frac{(1-c_\theta)}{\theta^2}\widehat{\boldsymbol{\omega}}^2 \tag{3}$$

$$G(\theta) = \left(I + \frac{(1-c_\theta)}{\theta^2}\widehat{\boldsymbol{\omega}} + \frac{(\theta - s_\theta)}{\theta^3}\widehat{\boldsymbol{\omega}}^2 \right) \tag{4}$$

where s_θ, c_θ correspond to $\sin\theta.\cos\theta$ respectively. In case of pure translation

$$T(\boldsymbol{\xi}) = \begin{bmatrix} I & \boldsymbol{v} \\ \mathbf{0} & 1 \end{bmatrix}, \quad \text{where } \boldsymbol{\xi} = \begin{bmatrix} \mathbf{0} \\ \boldsymbol{v} \end{bmatrix} \tag{5}$$

We use the modeling framework introduced by Woods et al. for modeling the mechanism [17]. The key geometric and kinematic relationships are summarized here for completeness, as they form the basis for the analytical stiffness derivation developed in this work. Each mechanism consists of four node points, defined in the local body frame, where strings are attached, Fig. 2. Let the number of nodes and string connections be $N_n = 4$ and $N_c = 12$, respectively. Define the node matrix

$$P = [\bar{\boldsymbol{p}}_a, \bar{\boldsymbol{p}}_b, \bar{\boldsymbol{p}}_c, \bar{\boldsymbol{p}}_d] \in \mathbb{R}^{4\times N_n}, \tag{6}$$

where $\bar{\boldsymbol{p}}_i = \left[\boldsymbol{p}_i^T, 1\right]^T \in \mathbb{R}^{4\times 1}$ is the homogeneous representation of node $\boldsymbol{p}_i \in \mathbb{R}^{3\times 1}$.

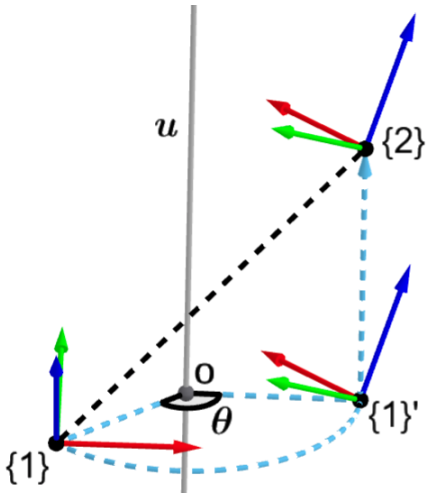

Fig. 1. Screw coordinate representation of the relative displacement between sub-vertebrae $\{1\}$ and $\{2\}$. The transformation $T(\boldsymbol{\xi}) = \exp(\widehat{\boldsymbol{\xi}})$ corresponds to a finite screw motion with $\boldsymbol{\xi} = [\boldsymbol{\omega}^T \ \boldsymbol{v}^T]^T$, where $\boldsymbol{u} = \boldsymbol{\omega}/\theta$ defines the screw axis and θ determines the motion magnitude. The origin of $\{2\}$ traces the associated screw trajectory shown.

The connectivity between the nodes and strings is described by a matrix $C_i \in \{0,1\}^{N_n \times N_c}$ for each sub-vertebra, where entry $C_i[j,k] = 1$ if string k is connected to node j, and zero otherwise.

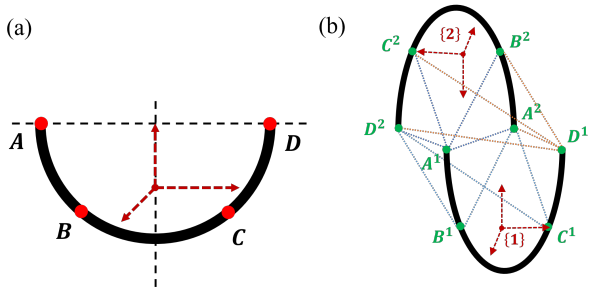

Fig. 2. Tensegrity mechanism comprising (a) the four node interaction points A, B, C, and D, and (b) the two curved links attached by 12 connection strings. The coordinate systems $\{1\}$ and $\{2\}$ are related by the screw $\boldsymbol{\xi}$. [17]

The string displacement matrix is defined as

$$\begin{aligned} S &= PC_1 - T(\boldsymbol{\xi})PC_2, \\ \bar{\boldsymbol{s}}_j &= \mathrm{col}_i(S) = \bar{\boldsymbol{p}}_i - T(\boldsymbol{\xi})\bar{\boldsymbol{p}}_j, \quad l_j = \|\boldsymbol{s}_j\|. \end{aligned} \tag{7}$$

where $S \in \mathbb{R}^{4\times N_c}$; j-th column of S $\bar{\boldsymbol{s}}_j$, is the displacement vector of the j-th string; and l_j is the instantaneous length of the string

Each string exhibits piecewise compliance modeled as

$$f_j = \begin{cases} 0 & l_j \le l_{0,j} \\ \dfrac{k_j(l_j - l_{0,j})}{l_j} & l_{0,j} < l_j < l_{\max,j} \\ \dfrac{k_j(l_{\max,j} - l_{0,j})}{l_j} & l_j = l_{\max,j} \end{cases} \tag{8}$$

where k_j is the linear stiffness, $l_{0,j}$ is the free length, and $l_{\max,j}$ is the maximum extension of string j.

The resulting forces in the strings and wrench acting on the mechanism is

$$\boldsymbol{\mathcal{F}} = \sum_{j=1}^{N_c} \boldsymbol{\mathcal{F}}_j \text{ s.t. } \boldsymbol{\mathcal{F}}_j = \begin{bmatrix} \sum_{j=1}^{N_c} \boldsymbol{f}_j \\ \sum_{j=1}^{N_c} \widehat{\boldsymbol{r}}_j \boldsymbol{f}_j) \end{bmatrix}, \boldsymbol{f}_j = f_j \boldsymbol{s}_j \tag{9}$$

where $\boldsymbol{r}_j$ is the position vector to the attachment point of string j, and $\wedge : \mathbb{R}^{3\times 1} \to \mathfrak{so}(3)$ in this scenario (also used previously for $\mathfrak{se}(3)$ map). For clarity, Tab. I summarizes the primary notation used throughout the analytical derivations.

TABLE I
SUMMARY OF NOTATION

Rigid Body Kinematics	
$\boldsymbol{\xi} = [\boldsymbol{\omega}^T \ \boldsymbol{v}^T]^T$	Screw coordinates
$\boldsymbol{\omega} \in \mathbb{R}^3$	Rotation vector
$\boldsymbol{v} \in \mathbb{R}^3$	Translational component of screw
$\theta = \|\boldsymbol{\omega}\|$	Rotation magnitude
$\widehat{(\cdot)}$	$\mathbb{R}^6 \to \mathfrak{se}(3)$ or $\mathbb{R}^{3\times 1} \to \mathfrak{so}(3)$
$T(\boldsymbol{\xi}) \in SE(3)$	Homogeneous transformation matrix
$G(\theta)$	Left Jacobian of $SO(3)$
Tensegrity Geometry	
$\boldsymbol{s}_j$	String direction/displacement vector
$l_j = \|\boldsymbol{s}_j\|$	Length of string j
l_0	Rest length of string
$\boldsymbol{r}_j$	Position vector of string attachment
Forces and Wrenches	
f_j	Scalar elastic force in string j
$\boldsymbol{f}_j = f_j \boldsymbol{s}_j$	Vector force applied by string j
$\boldsymbol{\mathcal{F}}_j$	Body wrench from string j
$\boldsymbol{\mathcal{F}}$	Total body wrench
Analytical Derivations	
$K = \partial\boldsymbol{\mathcal{F}}/\partial\boldsymbol{\xi}$	Joint stiffness matrix
$\partial T/\partial\boldsymbol{\xi}$	Transformation derivative tensor

III. Derivation of the Stiffness Matrix

The stiffness matrix $K \in \mathbb{R}^{6\times 6}$ of a tensegrity joint characterizes how small perturbations in the screw coordinates $\boldsymbol{\xi}$ produce changes in the body wrench $\boldsymbol{\mathcal{F}}$.

$$K = \frac{\partial \boldsymbol{\mathcal{F}}}{\partial \boldsymbol{\xi}} = \sum_{j=1}^{N_c} \frac{\partial \boldsymbol{\mathcal{F}}_j}{\partial \boldsymbol{s}_j} \frac{\partial \boldsymbol{s}_j}{\partial \boldsymbol{\xi}} = \left(\begin{bmatrix} I \\ \widehat{\boldsymbol{r}}_j \end{bmatrix} \frac{\partial \boldsymbol{f}_j}{\partial \boldsymbol{s}_j} \right) \frac{\partial \boldsymbol{s}_j}{\partial \boldsymbol{\xi}}. \tag{10}$$

Conceptually, this derivative measures how a perturbation in joint configuration propagates through the string geometry and alters the resulting body wrench. Each string j contributes a wrench: where $\boldsymbol{s}_j$ is the string direction vector and f_j is the scalar elastic force. This expression separates the stiffness into two effects of how : (i) string forces change with string displacement, capturing the local stiffness of an individual string, and (ii) how string displacements change with joint

Fig. 3. (left) Front and (right) Back view of the tensegrity sub-vertebra with compressive members and tensile connection strings.

configuration. Using (7), (8) and considering the string to be in the elastic region.

$$\frac{\partial \boldsymbol{f}_j}{\partial \boldsymbol{s}_j} = k_j \left(\frac{2l_0 - l_j}{l_j^4}\right) \boldsymbol{s}_j \boldsymbol{s}_j^T + k_j \frac{l_j - l_0}{l_j^2} I$$
$$\frac{\partial \boldsymbol{s}_j}{\partial \boldsymbol{\xi}} = -\frac{\partial T(\boldsymbol{\xi})}{\partial \boldsymbol{\xi}} \bar{\boldsymbol{p}}_j. \tag{11}$$

Therefore, the stiffness matrix is fully determined once the derivative of the transformation matrix with respect to its screw coordinates is known.

IV. Derivative of the Transformation Matrix

The derivative $\partial T/\partial \boldsymbol{\xi}$ is a $4 \times 4 \times 6$ tensor whose first three components correspond to $\boldsymbol{\omega}$ and the last three to $\boldsymbol{v}$. Structurally, each slice of this tensor describes how a small perturbation in one component of the screw modifies the rigid-body transformation.

A. Derivative with Respect to Rotation Parameters

Using (2), (3), and (4),

$$\frac{\partial T}{\partial \omega_i} = \begin{bmatrix} \frac{\exp(\widehat{\boldsymbol{\omega}})}{\partial \omega_i} & \frac{\partial (G(\theta)\boldsymbol{v})}{\partial \omega_i} \\ 0 & 0 \end{bmatrix}, \quad \text{for } i = 1, 2, 3 \tag{12}$$

Here, the derivative of the rotation matrix with respect to its screw coordinates admits the closed-form expression derived by Gallego and Yezzi [18]

$$\frac{\partial \exp(\widehat{\boldsymbol{\omega}})}{\partial \omega_i} = \frac{1 - c_\theta}{\theta^2} \left(\boldsymbol{e}_i \boldsymbol{\omega}^T + \boldsymbol{\omega} \boldsymbol{e}_i^T - \frac{2\omega_i \boldsymbol{\omega} \boldsymbol{\omega}^T}{\theta^2}\right)$$
$$\left(\frac{c_\theta \widehat{\boldsymbol{\omega}}}{\theta^2} + \frac{s_\theta \widehat{\boldsymbol{\omega}}^2}{\theta^3}\right) \omega_i + \frac{s_\theta}{\theta} \left(\boldsymbol{e}_i - \frac{\omega_i \boldsymbol{\omega}}{\theta^2}\right)^\wedge \tag{13}$$

where $\boldsymbol{e}_i = \mathrm{col}_i(I)$ is the i-th standard basis vector.

The derivative of the translation component requires differentiating the left Jacobian (4)

$$G(\theta) = I + b(\theta)\widehat{\boldsymbol{\omega}} + c(\theta)\widehat{\boldsymbol{\omega}}^2,$$
$$\text{where} \quad b(\theta) = \frac{1 - \cos\theta}{\theta^2}, \quad c(\theta) = \frac{\theta - \sin\theta}{\theta^3}. \tag{14}$$

Hence,

$$\frac{\partial G}{\partial \omega_i} = \left(\frac{\partial b}{\partial \theta}\right)\left(\frac{\partial \theta}{\partial \omega_i}\right)\widehat{\boldsymbol{\omega}} + b\frac{\partial \widehat{\boldsymbol{\omega}}}{\partial \omega_i}$$
$$+ \left(\frac{\partial c}{\partial \theta}\right)\left(\frac{\partial \theta}{\partial \omega_i}\right)\widehat{\boldsymbol{\omega}}^2 + c\left(\frac{\partial \widehat{\boldsymbol{\omega}}}{\partial \omega_i}\widehat{\boldsymbol{\omega}} + \widehat{\boldsymbol{\omega}}\frac{\partial \widehat{\boldsymbol{\omega}}}{\partial \omega_i}\right). \tag{15}$$

where

$$\frac{\partial \theta}{\partial \omega_i} = \frac{\partial \sqrt{\boldsymbol{\omega}^T \boldsymbol{\omega}}}{\partial \omega_i} = \frac{1}{\sqrt{\boldsymbol{\omega}^T \boldsymbol{\omega}}} \boldsymbol{\omega}^T \frac{\partial \boldsymbol{\omega}}{\partial \omega_i} = \frac{\omega_i}{\theta},$$
$$\frac{\partial b}{\partial \theta} = \frac{\theta s_\theta + 2c_\theta - 2}{\theta^3}, \frac{\partial c}{\partial \theta} = \frac{3s_\theta - \theta c_\theta - 2\theta}{\theta^4} \tag{16}$$

The matrices $\partial\widehat{\widehat{\boldsymbol{\omega}}}/\partial\omega_i = \widehat{\boldsymbol{e}}_i$ are constant skew-symmetric basis matrices. Therefore,

$$\frac{\partial (G(\theta)\boldsymbol{v})}{\partial \omega_i} = \left(\frac{\partial G(\theta)}{\partial \omega_i}\right)\boldsymbol{v}, \tag{17}$$

yielding a fully analytical closed-form expression for the translation derivative.

B. Derivative with Respect to Translation Parameters

For the translation elements $\boldsymbol{v}$ of the screw $\boldsymbol{\xi}$

$$\frac{\partial T}{\partial v_i} = \begin{bmatrix} 0 & \mathrm{col}_i(G(\theta)) \\ 0 & 0 \end{bmatrix}. \tag{18}$$

Together, these expressions provide a complete analytical characterization of how infinitesimal screw perturbations modify rigid-body motion in $SE(3)$. This closed-form derivative enables direct computation of the stiffness matrix without resorting to numerical differentiation.

The MATLAB implementation used to compute the analytical derivatives and evaluate the stiffness matrix given in this work is available as open-source code at: https://github.com/robbiemonke/StiffnessMatrix/tree/main

V. Physical Interpretation of the Stiffness Matrix

Although Eq. (10) provides the analytical expression for the stiffness matrix, additional physical insight can be obtained by examining its structure. As the screw coordinates and body wrench each contain rotational and translational components, the stiffness matrix allows for multiple useful interpretations that highlight how perturbations in the joint's configuration produce forces and moments in the mechanism.

A. Block Form Interpretation

Since the screw coordinates are given by $\boldsymbol{\xi} = [\boldsymbol{\omega}^T \ \boldsymbol{v}^T]^T$ and the resulting body wrench by $\boldsymbol{\mathcal{F}} = [\boldsymbol{f}^T \ \boldsymbol{m}^T]^T$, the stiffness matrix $K = \partial\boldsymbol{\mathcal{F}}/\partial\boldsymbol{\xi}$ can be expressed in block form as

$$K = \begin{bmatrix} K_{f\omega} & K_{fv} \\ K_{m\omega} & K_{mv} \end{bmatrix}, \tag{19}$$

where each matrix block is of 3×3 dimension. This decomposition provides a useful physical interpretation of the stiffness of the joint. The block K_{fv} represents translational stiffness, relating translational perturbations of the joint to the resulting forces, while $K_{m\omega}$ represents rotational stiffness, relating rotational perturbations to the resulting moments. The off-diagonal blocks capture coupled stiffness behavior: $K_{f\omega}$ describes forces generated by rotational perturbations, while K_{mv} describes moments generated by translational perturbations.

For tensegrity joints, these coupling terms are particularly significant because the tensile members transmit forces at distributed points in directions varying with time that simultaneously influence both translation and rotation. As a result, the stiffness matrix often exhibits strong off-diagonal structure, reflecting the inherently coupled mechanics of the mechanism.

Fig. 4 illustrates how the magnitude of each stiffness block varies as the joint evolves through an extensional displacement from its equilibrium configuration. The Frobenius norm of each block provides a quantification of the stiffness of each component. In this example, the translational stiffness block K_{fv} stays relatively constant throughout the displacement, while the rotational stiffness $K_{m\omega}$ gradually decreases as the joint moves away from the equilibrium position. The two coupling blocks, $K_{f\omega}$ and K_{mv} remain non-zero highlighting the inherent coupling between the translation and rotation of the tensegrity structure.

B. Column Form Interpretation

The stiffness matrix can also be interpreted column-wise as

$$K = \begin{bmatrix} K_{\mathcal{F}\omega_1} & K_{\mathcal{F}\omega_2} & K_{\mathcal{F}\omega_3} & K_{\mathcal{F}v_1} & K_{\mathcal{F}v_2} & K_{\mathcal{F}v_3} \end{bmatrix}$$

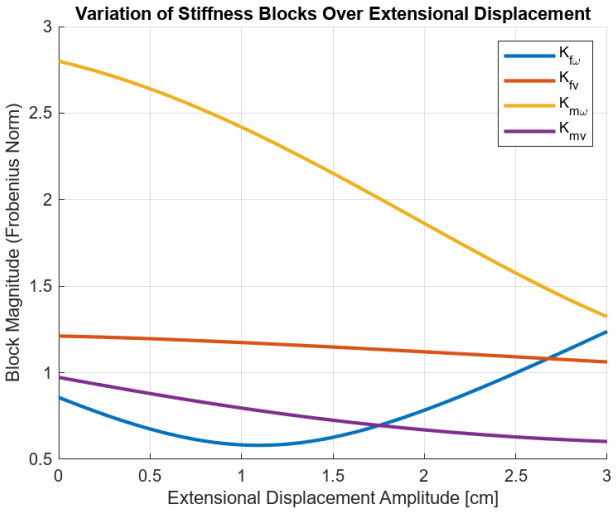

Fig. 4. Variation of the Frobenius norm of the stiffness matrix during an extensional displacement of the tensegrity joint. The block K_{fv} corresponds to a translational stiffness, $K_{m\omega}$ to a rotational stiffness, while $K_{f\omega}$ and K_{mv} represent the translation and rotation coupling.

where each column is a 6×1 vector representing the wrench generated by a perturbation in a specific screw coordinate. In this form, the i-th column describes how the body wrench changes given the corresponding screw coordinate ξ_i is perturbed. The magnitude of each column thereby defines which screw coordinate change produces the largest wrench back towards the joint's equilibrium position. This can be interpreted as the screw coordinate stiffness of the joint.

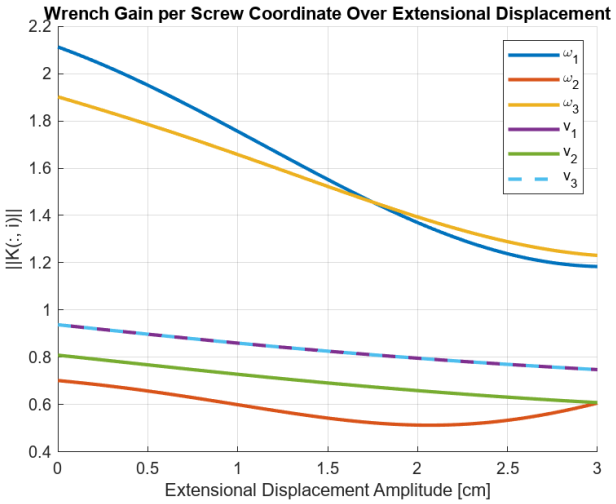

Fig. 5. Magnitude of each stiffness matrix column during an extensional displacement of the tensegrity joint.

Fig. 5 illustrates how the magnitude of each column of the stiffness matrix varies as the joint extends. At the equilibrium position, the columns corresponding to the rotational coordinates demonstrate the largest magnitude.

This indicates that small rotational perturbations will result in the largest restoring wrench. However, over the course of the extensional displacement, the decrease in the wrench gain from the rotational components demonstrates how the directional stiffness of the joint evolves with the configuration change.

C. Row Form Interpretation

The stiffness matrix can be interpreted row-wise as

$$K = \begin{bmatrix} K_{\xi f_1} \\ K_{\xi f_2} \\ K_{\xi f_3} \\ K_{\xi m_1} \\ K_{\xi m_2} \\ K_{\xi m_3} \end{bmatrix}, \tag{20}$$

where each row is a 1×6 vector describing how a particular component of the body wrench varies with changes in the screw coordinates. In this form, the j-th row represents the sensitivity of the wrench component $\mathcal{F}_j$ to perturbations in each component of the screw coordinate. This interpretation shows which motions most strongly influence a particular force or moment component. This allows for identification of how screw coordinate perturbations contribute to specific internal loading directions of the tensegrity joint.

VI. Results and Discussion

To validate the analytical expressions for the derivative of the transformation matrix, $T = \exp(\widehat{\boldsymbol{\xi}})$ in (12), (18), and the stiffness matrix, K in (10), they were compared against numerical differentiation using the central finite-difference method.

Let f denote either the transformation matrix, $T(\boldsymbol{\xi})$, or the wrench, $\mathcal{F}(\boldsymbol{\xi})$. Given a perturbation vector $\boldsymbol{\epsilon}$ with only the i^{th} component as nonzero, the numerical derivative with respect to ξ_i was computed as

$$\frac{\partial f}{\partial \xi_i}_{num} \approx \frac{f(\boldsymbol{\xi} + \boldsymbol{\epsilon}) - f(\boldsymbol{\xi} - \boldsymbol{\epsilon})}{2\,\epsilon_i}. \tag{21}$$

With the magnitude of the perturbation, ϵ_i, set to 10^{-6}, the relative error between the true analytical solution and the numerical differentiation is

$$\text{relative error} = \frac{\left|\left| \frac{\partial f}{\partial \xi}_{ana} - \frac{\partial f}{\partial \xi}_{num} \right|\right|_F}{\left|\left| \frac{\partial f}{\partial \xi}_{ana} \right|\right|_F} \tag{22}$$

where $\frac{\partial f}{\partial \xi_i}_{ana}$ and $\frac{\partial f}{\partial \xi_i}_{num}$ are the analytical and numerical derivatives, respectively. $||\cdot||_F$ symbolizes the Frobenius norm [19].

Using the energy minimization approach, 10000 stable configurations were found by randomizing the applied wrench to the joint and finding the corresponding minimum energy configuration screws. From these 10000 samples, the mean relative error for the stiffness matrix and derivative of the transformation matrix were calculated. The negligibly small values, 4.4333×10^{-10} and 2.4180×10^{-10}, respectively, demonstrate agreement to numerical precision and confirm that the results are identical.

TABLE II
Computational cost (avg of 10000 configurations)

Solution Type	$\partial \exp(\widehat{\boldsymbol{\xi}})/\partial \boldsymbol{\xi}$	Stiffness Matrix
Analytical	0.0843ms	0.3104ms
Numerical	0.2944ms	0.8394ms

Furthermore, the time to solve both the analytical solution and numerical differentiation was compared to demonstrate a benefit of the closed-form solution. The speed of the solver is particularly important in this application because of the ramifications in the ability to perform real-time control and state estimation of the tensegrity systems, e.g., manipulators. Both the numerical solution and the analytical solution were calculated using MATLAB 2024b and a computer with an Intel Xeon CPU E5-1650 v4 @ 3.60GHz and 64 GB RAM. The results tabulated in Tab. II show that the analytical solutions were approximately 3 times faster than their numerical counterparts, reducing average computation time from $0.2944ms, 0.8394ms$ to $0.0843ms, 0.3104ms$ for the transformation matrix derivative and stiffness matrix calculations, respectively for 10000 stable configurations. This computational advantage becomes even more significant when stiffness must be evaluated dynamically for multiple manipulator modules instead of a single module, where the cost of numerical differentiation can become prohibitive.

To further validate the derivation of the stiffness matrix, simulations were performed on the described mechanism where an external force was applied, the screw corresponding to the minimal energy state was found, and the corresponding body wrench was determined. Additionally, the screw and body wrench corresponding to the no load minimal energy state was found. When the screw and the body wrench of these two states were compared, the change in the screw of the system and the corresponding change in the body wrench were determined. Thereafter, the expected change in the wrench is calculated from the product of the stiffness matrix at the no load minimal energy state K and the change of screw. The simulated change in the body wrench and the change determined by the stiffness matrix were compared.

Two different perturbation forces were simulated to verify the response given by the stiffness matrix. A force was applied along the y-axis of the center of mass of the primitive to demonstrate the response to pure compression of the tensegrity joint, Fig. 6. The body wrench

TABLE III
BODY WRENCH RESPONSES FROM STIFFNESS MATRIX AND X, Y, AND Z PERTURBATION FORCES AT A2

Wrench responses to force at A2		
Force direction	Body Wrench	Relative Absolute Error
x	$\begin{bmatrix}0.0031 & -0.0073 & 0.0017 & 0.0053 & 0.0045 & 0.0025\end{bmatrix}^T$	0.26%
y	$\begin{bmatrix}0.0003 & 0.0035 & -0.0018 & -0.0015 & -0.0013\end{bmatrix}^T$	0.64%
z	$\begin{bmatrix}0.0076 & 0.0035 & -0.0070 & 0.0060 & 0.0015 & 0.0025\end{bmatrix}^T$	0.50%

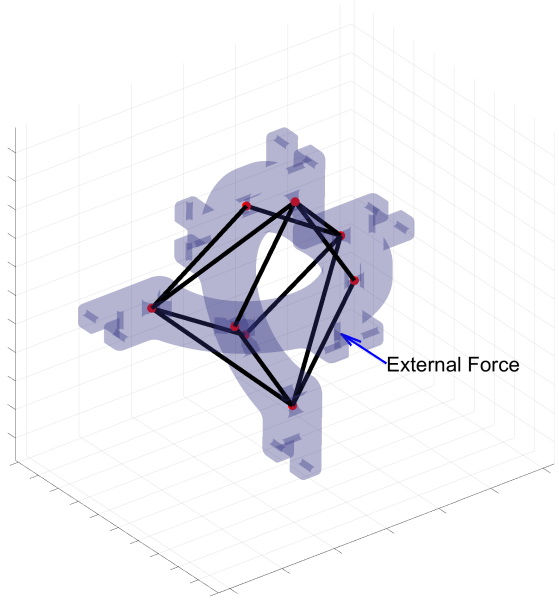

Fig. 6. Simulated response to compression of tensegrity sub-vertebrae.

response given by the stiffness matrix to the load was found to be $\delta\boldsymbol{\mathcal{F}} = \begin{bmatrix}0 & 0.0011 & 0 & 0 & 0 & 0\end{bmatrix}^T$. The comparison of the body wrench response found using simulation and the stiffness matrix for the compression load resulted in a relative absolute error of 0.17%. The compression test represents the simpler of the two loading scenarios in which translational displacement of the joint is observed independently of any rotational motion. This example provides an intuitive baseline for understanding the translational stiffness behavior of the tensegrity structure.

In addition to the compressive test, loads were applied in the x, y, and z directions respectively at node A2 to simulate the rotational response of the tensegrity joint; see Fig. 7. The body wrench responses given by the stiffness matrix to the load as well as the relative absolute error of the simulation can be found in Tab. III. Here, the relative errors in the three canonical directions are $0.26\%, 0.64\%$ and 0.50%. In contrast to the compression test, these rotational perturbations excite both the rotational and translation-rotation coupling, giving a more complete view of the joint behavior predicted by the stiffness matrix.

VII. CONCLUSION AND FUTURE WORKS

This work presented an analytical formulation for the stiffness matrix of tensegrity joints using a screw theory-based framework. By performing this derivation with respect to the screw coordinates, we derived a closed-form stiffness matrix that avoids the singularities and non-uniqueness associated with the Euler angle parameterizations. One key contribution of this work is the analytical solution of the derivative of the transformation matrix with respect to its screw coordinates, the screw $\boldsymbol{\xi}$. This formulation has not been seen in literature to this point. In addition to the analytical derivation, the stiffness matrix is interpreted in block, column, and row forms to expose its underlying physical structure. These representations clarify the translational, rotational, and coupled stiffness effects, and show how configuration perturbations map to the resulting wrench components.

The formulations proposed were validated through two approaches. First, comparisons with numerical differentiation showed agreement to within numerical precision, while computational times of 10000 different configurations show the analytical solution to be approximately 3 times faster than the numerical solution. Second, simulations of a tensegrity sub-vertebrae under compressive and rotational loads confirmed the stiffness matrix's ability to accurately predict the body wrench response of the system, with corresponding errors below 1%. Combined, these results verify the correctness, efficiency, and utility of the derived closed-form solutions.

Future work will focus include experimental validation will be performed on tensegrity joints to compare the solution to results under real-world conditions. Additionally, extension of the solution from single mechanism to multi-body tensegrity mechanisms will be explored. Second, compliance design of tensegrity sub-vertebrae will be performed to control the response of the joint to the expected perturbation forces to be applied to it. Finally, by extending the results of the derivative of the transformation matrix with respect to its screw coordinates into Euler-Lagrange dynamics, we look to develop a unified framework for the modeling of higher DOF tensegrity joints where all parameterizations are expressed consistently in screw coordinates.

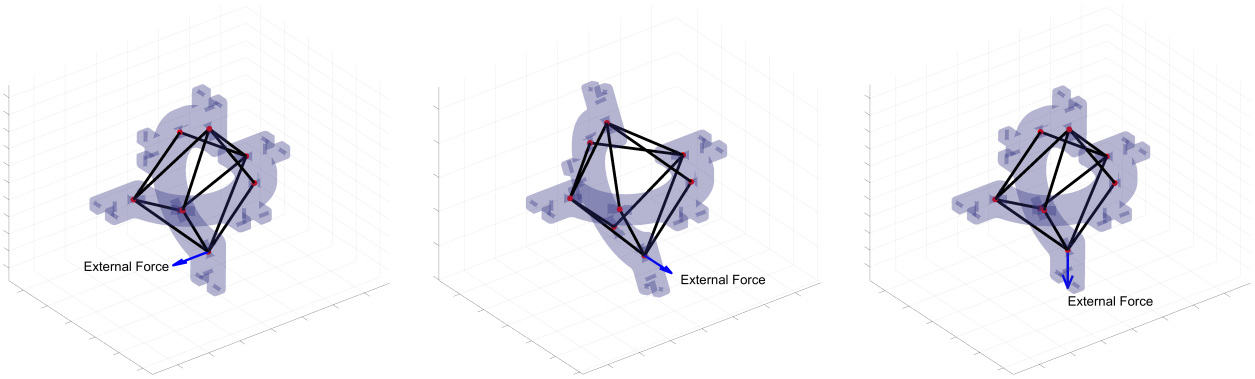

Fig. 7. Simulated response of tensegrity sub-vertebrae to perturbation forces at connection node: (left) force applied along x-axis, (middle) force applied along y-axis, and (right) force applied along z-axis

REFERENCES

[1] A. P. Sabelhaus, H. Ji, P. Hylton, Y. Madaan, C. Yang, A. M. Agogino, J. Friesen, and V. SunSpiral, "Mechanism Design and Simulation of the ULTRA Spine: A Tensegrity Robot," in *Volume 5A: 39th Mechanisms and Robotics Conference*, (Boston, Massachusetts, USA), p. V05AT08A059, American Society of Mechanical Engineers, Aug. 2015.

[2] M. C. Oliveira and R. E. Skelton, *Tensegrity Systems*. Boston, MA: Springer US, 2009.

[3] R. E. Skelton, R. Montuori, and V. Pecoraro, "Globally stable minimal mass compressive tensegrity structures," *Composite Structures*, vol. 141, pp. 346–354, May 2016.

[4] M. Vespignani, J. M. Friesen, V. SunSpiral, and J. Bruce, "Design of SUPERball v2, a Compliant Tensegrity Robot for Absorbing Large Impacts," in *2018 IEEE/RSJ International Conference on Intelligent Robots and Systems (IROS)*, pp. 2865–2871, Oct. 2018.

[5] S. Lessard, J. Bruce, E. Jung, M. Teodorescu, V. SunSpiral, and A. Agogino, "A lightweight, multi-axis compliant tensegrity joint," in *2016 IEEE International Conference on Robotics and Automation (ICRA)*, (Stockholm, Sweden), pp. 630–635, IEEE, May 2016.

[6] Y. Hao, J. Dai, Z. Jiang, A. P.-W. Lee, J. Lam, and K.-W. Kwok, "A Controllable-Stiffness Tensegrity Robot Joint for Robust Compliant Manipulation," *Journal of Field Robotics*, vol. 42, no. 7.

[7] Y. Hao, X. Wang, X. Song, Y. Li, H. Fu, A. P.-W. Lee, K. M.-C. Cheung, J. Lam, and K.-W. Kwok, "A Tensegrity Joint for Low-Inertia, Compact, and Compliant Soft Manipulators," *Advanced Intelligent Systems*, vol. 6, no. 2, p. 2300079, 2024.

[8] B. Chen, H. Jiang, J. Liu, and S. Lu, "Joint Equivalence Design and Analysis of a Tensegrity Joint," *Journal of Mechanisms and Robotics*, vol. 13, May 2021.

[9] L.-Y. Zhang, Y. Li, Y.-P. Cao, and X.-Q. Feng, "Stiffness matrix based form-finding method of tensegrity structures," *Engineering Structures*, vol. 58, pp. 36–48, Jan. 2014.

[10] S. Savin, O. Balakhnov, and A. Klimchik, "Convex Optimization-based Stiffness Control for Tensegrity Robotic Structures," in *2020 28th Mediterranean Conference on Control and Automation (MED)*, pp. 990–995, Sept. 2020.

[11] S. D. Guest, "The stiffness of tensegrity structures," *IMA Journal of Applied Mathematics*, vol. 76, pp. 57–66, Feb. 2011.

[12] M. Arsenault, "Stiffness Analysis of a 2DOF Planar Tensegrity Mechanism," *Journal of Mechanisms and Robotics*, vol. 3, Apr. 2011.

[13] R. M. Murray, Z. Li, and S. S. Sastry, *A Mathematical Introduction to Robotic Manipulation*. CRC Press, 1 ed., Dec. 2017.

[14] K. M. Lynch and F. C. Park, *Modern Robotics: Mechanics, Planning, and Control*. Cambridge University Press, 1 ed., May 2017.

[15] E. Minguzzi, "A geometrical introduction to screw theory," *European Journal of Physics*, vol. 34, pp. 613–632, May 2013.

[16] Y. Wang, J. He, X. Li, Y. Gao, and H. Jiang, "Dynamics for tensegrity structures based on screw theory," *Mechanism and Machine Theory*, vol. 214, p. 106129, Oct. 2025.

[17] C. Woods and V. Vikas, "Design and Modeling Framework for DexTeR: Dexterous Continuum Tensegrity Manipulator," *Journal of Mechanisms and Robotics*, vol. 15, p. 031006, June 2023.

[18] G. Gallego and A. Yezzi, "A compact formula for the derivative of a 3-D rotation in exponential coordinates," *Journal of Mathematical Imaging and Vision*, vol. 51, pp. 378–384, Mar. 2015. arXiv:1312.0788 [cs].

[19] T. A. Bui, J.-S. Kim, and J. Park, "Efficient Method for Derivatives of Nonlinear Stiffness Matrix," *Mathematics*, vol. 11, p. 1572, Jan. 2023.